Metal-organic frameworks for the capture of dissolved CO$_2$ and generated carbonate ions from water

Stefan Wuttke (✉ stefan.wuttke@bcmaterials.net)
BCMaterials, Basque Center for Materials   https://orcid.org/0000-0002-6344-5782

Jacopo Andreo
BCMaterials

Subhajit Dutta
BCMaterials, Basque Center for Materials

Nagore Barroso
BCMaterials, Basque Center for Materials

Aleksander Ejsmont
Adam Mickiewicz University

Bettina Baumgartner
Utrecht University

Agata Jankowska
Adam Mickiewicz University

Jonas Tittel
Ludwig-Maximilians-Universität München

Rafael Marcé
Catalan Institute for Water Research (ICRA)   https://orcid.org/0000-0002-7416-4652

Marcin Frankowski
Adam Mickiewicz University

Bert M. Weckhuysen
Utrecht University   https://orcid.org/0000-0001-5245-1426

Evelyn Ploetz
Ludwig-Maximilians-Universität München

Joanna Goscianska
Adam Mickiewicz University   https://orcid.org/0000-0002-4202-652X

Article

Keywords:

Posted Date: February 2nd, 2024

DOI: https://doi.org/10.21203/rs.3.rs-3353195/v1

Additional Declarations: There is **NO** Competing Interest.

Abstract

Anthropogenic CO_2 emissions are the major driver of climate change of this century. The natural hydrological cycles cause atmospheric CO_2 to be absorbed by the natural water bodies, which necessitates urgent removal of dissolved CO_2 and their generated carbonate species from water. Herein, we report the first benchmark study to explore the potentials of the highly porous hybrid material class of metal-organic frameworks (MOFs) for the effective removal of dissolved CO_2 and carbonic acid species from water. Seven diverse MOFs with a wide range of structural, and compositional varieties were selected on the basis of their gaseous phase CO_2 capture performance. Single component adsorption studies revealed remarkably diverse CO_2 removal performances, highlighting key roles of the pH (e.g., 2, 6.3, 8.3, and 10) and the nature of the carbonic species present. Amongst all materials, JUK-8 exhibited the highest adsorption capacity of 6.79 mmol/g toward carbonic acid species at pH 6.3 (CO_2 and HCO_3^-). Importantly, the MOFs were also found to exhibit substantial removal performance while tested with diverse natural water samples.

Introduction

Over the past 250 years, levels of the most abundant greenhouse gas on earth, carbon dioxide (CO_2), have increased by ~ 50% compared to the pre-industrial era essentially due to human fossil fuel combustion and deforestation[1,2]. While the atmospheric CO_2 level was about ~ 280 ppm in the 1800s, it recently rose to over ~ 400 ppm and is projected to reach ~ 950 ppm by 2100[3−5]. Anthropogenic CO_2 emissions have resulted in (and will continue to cause) serious environmental problems like global warming, ocean acidification, melting of snow cover and ice caps, elevated sea levels, and species extinction[6,7]. Natural hydrological cycles cause atmospheric CO_2 to be taken up by the ocean and other bodies of water[8−10]. Consequentially, about 30 % of the caron that humans released into the atmosphere has been absorbed by the oceans; without this sink, atmospheric CO_2 levels would be nearly at 450 ppm today. CO_2 absorption significantly modifies ocean chemistry, leading to reduced pH levels and fundamental changes in seawater carbonate chemistry, often referred to as "other CO_2 problems"[11,12]. Since the 1950, the pH of the oceans' surface has experienced a decrease of approximately 0.1, a change ten times faster than any other occurrence estimated in the last 300 million years. Consequently, the oceans are experiencing unprecedented catastrophes like marine heat waves, coral-bleaching, widespread habitat destruction, and ocean acidification (Fig. 1)[13,14].

Carbon capture and storage (CCS) is widely accepted as a critical part of any solution to reverse the effects of climate change, and a great deal of technologies have been developed to perform this task[7,15−17]. CO_2 capture methods include adsorption (physisorption and chemisorption), physical/chemical absorption, cryogenic fractionation, and membrane-based separation. Among these, physisorption with porous materials is perhaps the most efficient method, with a much smaller energy footprint than any of

the others[18,19]. Notably, most of the CCS methods and technologies are established to tackle gas phase CO_2, rendering a huge scientific and technological gap in CCS from liquid phase.

Over the last two decades, metal-organic frameworks (MOFs) have been designed and optimized specifically for gas capture, including atmospheric CO_2 (Fig. 1)[20–23]. Of all of the adsorbents available today, MOFs stand out as particularly advantageous, with high surface areas, compositional diversity, tailorable pore functionalization, and installation of selective functional groups[24–27]. As a consequence, they have become popular sorbent materials and have been widely studied[1,28,29] for the capture of different gas molecules, including volatile organic compounds[30], hydrogen[31], methane[32], and CO_2[33] as well as common water pollutants like dyes[34], heavy metal ions[35], and pharmaceuticals[36]. MOFs have broken records for CO_2 gas capture and storage (Supplementary Table S2.1) from the gas phase. Surprisingly, despite the excellent performance of these materials toward CO_2 capture and their reliable performance in aqueous environments for other applications, MOFs have never been utilized for CO_2 removal from aqueous environments (Fig. 1). This creates a serious scientific knowledge gap and a window of opportunities for both chemical and material scientists to introspect the area of aqueous CO_2 sequestration by such materials.

In this contribution, we present a first study that explores the potential of various MOF systems for capturing dissolved CO_2 and other carbonate species from water to provide a possible solution to increasing CO_2 uptake by the oceans. Seven representative MOFs were selected, which were extensively studied for CO_2 capture in the gas phase before. The MOFs were selected according to their high adsorption capacity, such as MIL-127(Fe)[37], Cu-TDPAT[38], MOF-74 (Ni)[39], UiO-66(Zr)[40,41], UiO-66-NH$_2$(Zr)[41] and JUK-8(Zn)[42], or high selectivity (ZU-301(Zn)[43]), while providing a broad selection of material properties simultaneously such as chemical composition, structure, porosity, and functionality. The single-component adsorption study revealed diverse sorption behavior of different MOFs at different pH levels and toward different carbonic acid species. The sorption behavior of the MOFs toward carbonic acid species was also tested in several real-world water samples (e.g., Pletera Lagoon, Foix Reservoir, Colomers Weir, Mediterranean Sea, and Tordera River) to test their potential toward rational mitigation of dissolved CO_2 in water bodies. Further, *in situ* vibrational spectroscopic results revealed key mechanistic insights regarding the adsorption process and differential properties between CO_2(g) and CO_2(l) phase.

Results

CO_2 and carbonic acid species in water.
Carbonic acid is a diprotic acid that converts into different forms depending on the pH (pH = 2–10)[44]. In acidic conditions, the dominant form is CO_2, while under basic conditions, the majority remains as carbonate anions (CO_3^{2-}). The intermediate pH ranges are dominated by the bicarbonate anions (HCO_3^-). It should be noted that the concentration of carbonic acid is found to be negligible compared to the concentration of the other carbonate species in all pH ranges.

Hence, to study the adsorption behavior of MOF materials towards CO_2 capture in water, four different pH values namely, pH 2, 6.3, 8.3, and 10 were selected. These were chosen according to the dominant species, which are CO_2, CO_2/HCO_3^-, HCO_3^-/CO_3^{2-} and CO_3^{2-}, respectively (for details see Supplementary Note 2.1).

MOFs selection criterion. The primary selection criterion for the MOFs was a good track record of CO_2 adsorption in the gas phase (Supplementary Note 2.2), which will allow us to compare and correlate their adsorption phenomenon depending upon the matrix (air and water). Moreover, careful consideration was given to selecting MOFs that exhibit a wide range of structural characteristics (different topology, porosity, structural flexibility, etc.) and chemical properties (presence of open metal sites, basic groups, etc.) in order to study their influence on the adsorption process. Seven MOFs were selected, which can be primarily categorized into two groups (Fig. 2): MOFs with high CO_2 adsorption capacity at the gas phase, namely MOF-74 (Ni), MIL-127, Cu-TDPAT, UiO-66, UiO-66-NH$_2$, and JUK-8, and MOFs with high selectivity toward CO_2, *i.e.* ZU-301 (Supplementary Figure S2.2)[33]. The six high-capacity MOFs can be further subdivided into three categories depending on the structural characteristics: *i*) MOFs with undercoordinated metal sites, *ii*) MOFs with basic groups and *iii*) MOFs with a flexible framework, all of them are well known to assist in high CO_2 uptake. MOF-74 (Ni), MIL-127, and Cu-TDPAT allow us to understand the role of open metal sites and different coordination environments in CO_2 capture from water. For example, the open metal sites of MOF-74 (Ni) are at the apical position of the coordination sphere, which is known to selectively interact with the incoming CO_2 molecules[50]. MIL-127 possesses a metal secondary building unit of trimeric iron(III) cluster, and coordinated chloride anion is easily exchangeable[51]. Cu-TDPAT presents a copper paddlewheel cluster, and the free apical position of the coppers is coordinated by an exchangeable DMF molecule[52]. UiO-66 and UiO-66-NH$_2$ were chosen as the representative well-studied, robust MOF and functionalized MOF with basic groups, which - in comparison - can highlight the role of basic groups toward CO_2 affinity. JUK-8 was selected as a flexible MOF, which allows us to understand the role of structural dynamics upon the incoming guest loading. For example, it is found to transform from its closed form to open form in the presence of water or carbon dioxide, which makes it interesting and promising to study this MOF for CO_2 capture in water. On the other hand, ZU-301 has an optimum pore size and geometry to sieve molecules larger than CO_2, thus selectively adsorbing it over other small molecules[42].

Stability of the MOFs. Prior to evaluating their adsorption performance for different carbonate species in aqueous solutions, the stability of MOFs at the above-mentioned four pHs was monitored (Supplementary Note 4). For those experiments, all the MOFs were suspended in water at the corresponding pH solutions for 4 h, subsequently filtered and dried in air. Afterward, PXRD experiments elucidated their structural integrity (Supplementary Figure S4.1). All the MOFs exhibited good stability at pH 8.3 and pH 10, while higher acidity was found to result in structural instability. In particular, JUK-8 and Cu-TDPAT showed structural instability at pH 2, while ZU-301(Zn) showed structural instability at both pH 2 and 6.3. In addition, Cu-TDPAT exhibited partial instability during adsorption experiments at pH 6.3

depending on the carbonate concentration in the solution. This phenomenon can be correlated to the ability of carbonate ions to replace the carboxylate groups coordinating the copper paddlewheel in the MOF structure[45]. According to their stability performances, we further employed the MOFs for the adsorption studies in different pH conditions.

Uptake studies from water solutions. Adsorption experiments revealed remarkable differences in the MOF performances depending on the nature of carbonate species and the pH of the medium (Fig. 3; Supplementary Note 5). At pH 2, which contains only neutral species (CO_2 and H_2CO_3), MOFs with open metal sites exhibited the highest sorption capacity (of 4.00 mmol/g and 2.78 mmol/g for MOF-74 (Ni) and MIL-127, respectively, toward the dissolved species (Fig. 3a). On the contrary, UiO-66 and UiO-66-NH_2 showed much lower adsorption capacities of 0.84 mmol/g and 1.23 mmol/g, respectively. Moreover, the saturation concentrations ranged from 3.53 mmol/g for MIL-127 to 2.39 mmol/l for MOF-74 (Ni). It is worth noting that despite similarities between the species involved, the observed adsorption trend under these conditions differs significantly from the gas phase CO_2 adsorption behavior exhibited by these MOFs. Such variation in the adsorption performance can be attributed to several factors, such as solvation sphere formation or the presence of competing molecules.

At pH 6.3, at which both CO_2 and HCO_3^- are present, all MOFs discussed for pH 2 showed lower adsorption capacities. Interestingly, the well-performing MOFs (MOF-74 (Ni), MIL-127) at pH 2 showed comparatively lower adsorption capacities at pH 6.3. For instance, both MOF-74 (Ni) and MIL-127 showed a significantly reduced capacity of 0.36 mmol/g and 1.42 mmol/g, respectively, whereas UiO-66 and UiO-66-NH_2 registered an uptake capacity of 0.69 mmol/g and 0.90 mmol/g respectively. Such differential performance can be correlated with the presence of different carbonic species at this pH (Fig. 3b). Interestingly, JUK-8 stood out as the best-performing MOF at pH 6.3, with a staggering capacity of 6.79 mmol/g, corresponding to 30% in weight. Overall, all MOFs presented similar saturation concentration ranges, although the measured concentrations are lower at this pH compared to pH 2. The saturation concentrations for UiO-66 (3.15 mmol/g) and UiO-66-NH_2 (2.78 mmol/g) were slightly higher than for the MOF-74 (Ni) (2.11 mmol/g) and MIL-127 (2.53 mmol/g). JUK-8 showed a higher saturation concentration of 7.87 mmol/g. Notably, much higher CO_2 or carbonate concentrations were needed to reach the saturation capacity of JUK-8 compared to the other MOFs tested. In addition, the adsorption isotherm of JUK-8 at pH 6.3 showed multistep sorption behavior with a clear step around 3.5 mol/g of CO_2. This observation suggests a significant interaction between the incoming carbonate molecules and the MOF scaffold, resulting in potential structural alteration of the flexible JUK-8 structure. Consequently, JUK-8 can transform into three different possible pore-opening configurations (closed, partially and fully open) depending on the exposure matrix. In fact, the N_2 adsorption at 77 K shows the completely non-porous nature of the MOF, whereas water and CO_2 molecules are observed to contribute to opening the pores of JUK-8 (Supplementary Note 3.8)[42].

Adsorption studies at pH 8.3 revealed a similar trend as pH 6.3 for UiO-66, UiO-66-NH_2, and MOF-74 (Ni), with adsorption capacities of 0.64 mmol/g, 0.88 mmol/g and 0.33 mmol/g respectively (Fig. 3c). On the

contrary, MIL-127 and JUK-8 exhibited decreased removal capacities of 0.55 mmol/g and 0.63 mmol/g. Cu-TDPAT showed an adsorption capacity of 0.44 mmol/g, which is in line with the other open metal site MOFs. Following the trend, ZU-301 also showed lower uptake of only 0.17 mmol/g, which can be explained by the presence of smaller pores in ZU-301, rendering lower compatibility to accommodate the solvation sphere of the carbonate anions. Carbonate saturation studies revealed a general trend of the saturation in the range between 0.84 mmol/g for Cu-TDPAT and 1.63 mol/g for UiO-66, whereas JUK-8 showed a much higher carbonate saturation of 5.67 mmol/g.

At the most basic pH (pH 10), the species present in the solution are both HCO_3^- and CO_3^{2-}, and two distinct behaviors emerge in the materials. UiO-66, JUK-8, and ZU-301 revealed a decrease in adsorption capacity, while UiO-66-NH$_2$, MOF-74 (Ni), and MIL-127 showed an increment in their respective uptake capacities (Fig. 3d). In particular, UiO-66-NH$_2$ exhibited an exceptional removal capacity of 1.16 mmol/g, a double value from the next best-performing MOF at this pH. The preferential interaction between the incoming carbonate species with the dangled reactive NH$_2$ groups facilitated the removal process for UiO-66-NH$_2$. Cu-TDPAT was found to almost retain its performance, with a difference of less than 0.1 mmol/g in adsorption. Material saturation was reached at higher concentrations for almost all materials, except ZU-301 and JUK-8, for which it dropped to 1.70 mmol/l.

Overall, these results highlight several trends among the MOFs and the nature of the sorbate species (Fig. 3e). Among all the chosen MOFs, JUK-8 demonstrated the best adsorption performance (at pH 6.3) with the highest uptake capacity of 6.79 mmol/g. Alike other MOFs, JUK-8 was also found to perform better under acidic conditions than basic ones (pH 6.3 (6.79 mmol/g) > pH 8.3 (0.63 mmol/g) > pH 10 (0.47 mmol/g)). MOFs with open metal sites (MOF-74 (Ni), Cu-DTPAT, and MIL-127) showed a decreasing trend in CO_2 adsorption capacity from acidic to basic pH values. UiO-66 was also found to follow this trend with a less pronounced difference between the high and low pHs. ZU-301, featuring small pore-apertures, showed low or negligible adsorption performance. UiO-66-NH$_2$ consistently maintained its excellent adsorption capacity throughout all pH values.

Advanced material characterization by vibrational spectroscopy. Intrigued by the complex uptake behavior of carbonates by MOFs, we lastly asked how the adsorption process actually takes place on a molecular level. For this, we studied the two best-performing MOFs (UiO-66-NH$_2$ and JUK-8) via confocal imaging as well as *in situ* and spatially resolved vibrational spectroscopy. At first, we characterized both MOF materials in water using two-photon-excited fluorescence scanning microscopy (Fig. 4a; Supplementary Note S6.1) and investigated their morphology in water. In line with SEM imaging (Supplementary Figure S3.6), JUK-8 consists of large crystals of at least 50 μm with clean surfaces. UiO-66-NH$_2$ particles, however, are micron-sized aggregates assembled from nanoparticles 200−500 nm in diameter that disintegrate in water over time. Nanoparticles re-suspend into solution and, hence, provide both a large internal as well as external surface-to-volume ratio available for the adsorption of carbonates species.

Next, we aimed to investigate how CO_2 adsorption affects both frameworks at different pH values by vibrational spectroscopy. To assign host and guest associated signatures, we utilized IR and Raman spectroscopy to confirm the published chemical composition of all MOFs (Supplementary Note 6.2). In line with measurements by PXRD and TGA, both MOFs are stable shown by unaltered Raman spectra in air and water (Supplementary Note 6.3). For JUK-8, Raman spectroscopy additionally revealed that linker-associated modes in the fingerprint spectrum between $800-1600$ cm^{-1} change in amplitude. We tentatively assign these changes to the protonation of amine groups at basic pH and a local neutralization (Supplementary Figure S6.6). This finding could well explain the decreased binding of doubly negatively charged carbonate at pH 10 (Fig. 3d). Having confirmed that water also penetrates JUK-8 (Supplementary Note 6.4), we next benchmarked the vibrational signatures of CO_2 in water. While CO_2 is only visible by IR spectroscopy at 2345 cm^{-1}, the three different carbonate species are well distinguishable by both techniques (Supplementary Note 6.2.4). The short-lived carbonic acid was only visible at 1016 cm^{-1} under saturated conditions at pH = 10 via Raman spectroscopy but dissolved bicarbonate can be monitored via all three modes around 1005, 1300, and 1360 cm^{-1} with both techniques. Dissolved carbonate is best followed by IR spectroscopy at 1360 cm^{-1}.

For investigating the molecular uptake mechanism within both MOFs, we utilized *in situ* ATR-FTIR spectroscopy. We monitored the adsorption behavior of MOF-coated ATR crystals to probe the uptake kinetics (Fig. 4b). Experiments were carried out in a flow cell, which was initially filled with pure water only. Upon buffer exchange, new IR bands were observed for a 150 mmol/l solution of $NaHCO_3$ at pH 8.3 in comparison with the pristine MOFs (Supplementary Figure S6.3-6.5). Besides the emergence of new IR bands, the vibrational signature of $UiO-66-NH_2$ exhibited significant differences in the presence of $NaHCO_3$. Figure 4c shows the difference in IR spectra of $UiO-66-NH_2$ during buffer exchange. Negative bands around 1400 cm^{-1} and 1588 cm^{-1} appeared, which coincide with the carboxylate stretching modes of the amino terephthalic acid coordinated to the Zr-clusters. These bands are indicative of preferential interaction between the incoming HCO_3^- ions and the MOF scaffold, which is in strong contrast to the gas-phase CO_2 adsorption phenomenon of MOFs as such framework perturbation is never observed (Supplementary Note S6.5)[46]. It is noteworthy mentioning that a small band at 2345 cm^{-1} was observed corresponding to dissolved CO_2 together with a small shoulder around 2336 cm^{-1} which can be assigned to adsorbed CO_2. As it is typically reported for gas-phase CO_2 adsorption, this band is shifted to lower wavenumbers. The band completely vanished during the washing step with distilled water (Supplementary Note S6.6). Moreover, the significant broadening of the stretching vibrations of the carboxyl group around 1588 cm^{-1} ($v_{as}(COO^-)$) and 1383 cm^{-1} ($v_s(COO^-)$) and the appearance of a shoulder around 1340 cm^{-1} can be correlated with the structural change of the MOF structure. Bands of pristine $UiO-66-NH_2$ around 1408 cm^{-1} (multiple bands) and 1623 cm^{-1} correspond to an ammonium carboxylate salt that is formed during the synthesis using HCOOH as the modulator.[53] During the application of $NaHCO_3$, $HCOO^-$ is replaced by a carbonate species indicated by the appearance of bands at 1614 cm^{-1}, 1635 cm^{-1}, and 1692 cm^{-1} and a decrease of bands corresponding to the carboxylate.

The retention of both the negative and positive signatures at 1630 cm^{-1}, 1550 cm^{-1}, 1484 cm^{-1}, and 1330 cm^{-1} upon replacing of $NaHCO_3$ solution with pure water are indicative of the irreversible formation of ammonium carbonates with the amine group of UiO-66-NH_2 (Supplementary Note 6.3). Lastly, the bands associated with carbonate species between 1600–1700 cm^{-1} are found to be more prominent compared to liquid phase spectra (black trace), which suggests its enrichment inside the MOF pores[54].

Correspondent experiments were carried out for JUK-8 to understand the adsorption behavior toward carbonic acid species in water. As evident from Fig. 4d, in addition to bands associated with the $NaHCO_3$ solution at 1360 cm^{-1} and 1620 cm^{-1}, bands around 1275 cm^{-1}, 1400–1500 cm^{-1}, 1575 cm^{-1}, and 1660 cm^{-1} were observed for JUK-8 upon adding the 150 mmol/l $NaHCO_3$ solution. The bands around 1400–1500 cm^{-1} and 1660 cm^{-1} correspond to the polydentate CO_3^{2-} and HCO_3^- species, whereas bands around 1575 and 1274 cm^{-1} can be correlated with the bidentate CO_3^{2-} species[47–49]. This observation is not only a direct measure of intermolecular interaction between the incoming HCO_3^- ions and the Zn metal nodes of JUK-8 but also provides conformation about the *in situ* interactive species (*i.e.*, CO_3^{2-} and HCO_3^-). Moreover, the appearance of minor negative bands at 1245 cm^{-1} and 1597 cm^{-1} indicates an insignificant perturbation of the MOF during the adsorption process. Interestingly, JUK-8 exhibited lesser retention of the bands associated with carbonate species upon replacement of the HCO_3^- ions with pure water (Supplementary Note 6.5), which is in contrast to the structural changes associated with gas-phase CO_2 uptake where the stepwise CO_2 uptake results in stronger interaction and prominent structural change (Supplementary Note 6.6)[42]. This finding indicates that hydrogen bonding in JUK-8 due to water dominates alleviating contributions by charged guest molecules on the framework. In the gas phase, only interactions between CO_2 and the framework affect the structure as CO_2 binds preferably to an empty framework (Supplementary Note 6.7).

Knowing that CO_3^{2-} and HCO_3^- ions interact with both frameworks, the sorption kinetics was consecutively evaluated via filling the flow chamber with 150 mmol/l $NaHCO_3$ at pH 8.3. The carbonate solution was quantified as a function of time via monitoring the IR band corresponding to dissolved $NaHCO_3$ at 1362 cm^{-1}. As evident in Fig. 4e, the saturation concentration was reached within less than 2 minutes for the ATR crystals. The delay in kinetics compared to the reference measurement with the empty cell, can be correlated with the continuous uptake of the carbonic acid species during flushing. Both MOFs exhibited a nearly identical, temporal profile as the IR signature reaches the saturation level.

Overall, vibrational spectroscopic findings evidently confirmed the ability to adsorb carbonic acid species from water for both JUK-8 and UiO-66-NH_2 frameworks while involving strikingly different molecular mechanisms. ATR-FTIR investigation identified the presence of various carbonate species and revealed a strong difference in the uptake composition for both frameworks, which can be attributed to their differences in overall structural composition. While UiO-66-NH_2 incorporates even traces of gaseous CO_2, its linkers preferably interact with HCO_3^- ions and irreversibly form ammonium carbonates. In contrast,

JUK-8's uptake capabilities rely on interactions with the Zn-metal node, leading to the uptake of various carbonate species only, including both CO_3^{2-} and HCO_3^- species.

MOF chemistry: CO$_2$ (gas) vs CO$_2$ (liquid). It is well recognised that gas phase CO_2 adsorption operates via electrostatic interactions between incoming CO_2 molecules and the MOF frameworks (Fig. 4f). For instance, UiO-66-NH$_2$ interacts with CO_2 molecules via pendent -NH$_2$ groups and Zr-metal cluster-bound OH-groups (Fig. 4f, S6.13). The adequate balance between polar functional groups and hydrophobicity of the pore surfaces was found to play key roles in CO_2 adsorption from air[55]. Particularly, hydrophobic MOFs have shown excellent CO_2 adsorption in gas phase even under humid conditions as the hydrophobicity can restrict the competing water molecules and improve CO_2 uptake[56]. Conversely, transitioning CO_2 from gaseous to liquid phase involves a transformation in molecular-level chemistry, where the dissolved CO_2 molecules are present mainly as anions in the form of CO_3^{2-} and HCO_3^- (Fig. 4f). The ionic nature of these species induces strong coulombic interactions between the incoming species and the host framework, as evident from the *in situ* spectroscopic studies (Fig. 4)[57]. Thus, the liquid phase adsorption process involves both coulombic and electrostatic interactions between the anionic species and the host framework. Moreover, the adsorption trends indicate that adsorption capacity of the MOFs drops from acidic to basic pH which can be attributed to the introduction of higher competing species (e.g., OH^-) with increasing pH (Fig. S5.2a). In contrast to the gas phase, higher degree of hydrophobicity can be disadvantageous for adsorption from the liquid phase as it can restrict the water flow and hence the adsorption process. As the interaction of charged guest molecules can affect both structural flexibility and pore opening a thorough investigation of diverse MOF systems will be required in the future to benchmark different MOFs among each other in terms of their uptake capacity, selectivity, and kinetics.

Real-world sample testing. Adsorption performance in real-world complex matrixes is one of the crucial criteria to evaluate the potential of any sorbent materials. Encouraged by the above-mentioned results, we decided to carry out the first proof-of-concept studies and investigated whether CO_2 removal from real-world water samples, collected from lakes, rivers, and the Mediterranean Sea (areas in eastern Spain, Supplementary Note 7) can be monitored via MOFs. Different natural water bodies consist of diverse chemical constituents such as dissolved gases (e.g., CO_2 and O_2), inorganic ions, and organic compounds. Hence, this set of experiments is not to be intended as a direct applicability of MOFs as adsorbers for water-solubilized carbon capture, but as a preliminary way to gauge the material behavior in more complex matrixes. To cover a wide range of inorganic carbon species concentrations and water alkalinity, the water samples were collected from diverse natural sources in Spain: the Pletera Lagoon, Foix Reservoir, Colomers Weir, the Mediterranean Sea, and the Tordera River. Next adsorption experiments via high-temperature combustions were carried out to quantify the total inorganic carbon (TIC) concentration (in mmol/l), together with the pH value, alkalinity, and electric conductivity of the natural water samples.

Strikingly, the sample with the highest inorganic carbon concentration, *i.e.*, Pletera Lagoon water, is also found to be the most alkaline and conducting, while the Mediterranean Sea sample showed a large exception in conduction values because of its´ high salinity (Supplementary Table S7.1). The adsorption experiments revealed an interesting trend in the efficiency of the MOFs in the TIC removal (Fig. 5; Supplementary Table S7.3). MIL-127, Cu-TDPAT, UiO-66 and UiO-66-NH_2 exhibited excellent overall removal efficiencies even in samples with lower TIC concentrations. The removal efficiencies of these MOFs were found to be in between 9% -23% for the Pletera Lagoon (eq. concentration of HCO_3^-: 4.73 mmol/l), and 19%-30% for the Foix Reservoir (3.90 mmol/l) which are in agreement with the single component sorption performances. On the other hand, the adsorption performance with the lower TIC content, i.e., Colomers Weir (2.50 mmol/l) and the Mediterranean Sea (2.11 mmol/l) found to follow a similar trend as MIL-127 registered removal efficiencies of 38% and 40% respectively whereas Cu-TDPAT showed removal efficiencies of 38% and 41% respectively. Interestingly, UiO-66 and UiO-66-NH_2 exhibited enhanced efficiency toward the Mediterranean Sea sample (28% and 39% respectively) in comparison with the Colomers Weir samples (19% and 30% respectively). This improvement can be corelated with the lower competition of water for the materials adsorption sites. The higher concentration of ions in the sea sample (sodium and chloride ions), forces the water molecules in solvation spheres and thus lowering their availability to enter the pores and weakening the solvation spheres of the carbonic species simultaneously, allowing an easier adsorption. In addition, MIL-127, Cu-TDPAT, UiO-66, and UiO-66-NH_2 exhibited a considerable adsorption efficiency between 31%-59% toward the Tordera River sample with the lowest TIC (0.95 mmol/l).

Surprisingly, MOF-74 (Ni), JUK-8, and ZU-301 were found to exhibit lower adsorptions for the real-world samples. In particular, MOF-74 (Ni) presented a very low adsorption only for the three samples with the higher TIC concentrations, while negligible adsorption was detected for the Mediterranean Sea and the Tordera River samples. JUK-8 presented negligible adsorption for the Pletera lagoon sample, while its efficiency for the other four varied between 1–9%. ZU-301 was able to adsorb small amounts of TIC in all samples, with a maximum < 4% of the sample concentration. Most likely, the high affinity of JUK-8 and ZU-301 for CO_2 over HCO_3^- and CO_3^{2-}, allowed these MOFs to adsorb only the dissolved gaseous CO_2 present in the sample.

Conclusion

In summary, we have demonstrated the first comprehensive study of MOFs for the removal of dissolved CO_2 and carbonates from water. Our strategical selection of a wide range of MOFs with structural and functional diversity found to be crucial in exploring and understanding the key insights regarding the adsorption processes via functional porous materials in water and natural water samples. Single component adsorption experiments underlined the role of imperative parameters such as pH of the medium, nature of carbonic species, behaviour of diverse MOFs etc. toward the overall adsorption performance. Amongst all MOFs, JUK-8 exhibited the benchmark carbonate removal capacity at pH 6.3, whereas UiO-66-NH_2 was also found to retain its excellent adsorption efficiency over all pH ranges.

Although the adsorbent development is far from trivial, this extensive study allows us to grasp the key factors from both materials' designing and pH of the medium/ carbonic acid species perspective toward overall removal processes. For example, the physiochemical stability of the materials along with the adequate balance between structural porosity and functionality are of paramount importance which can render efficient carbonate species removal from water. In addition of the niche applicability toward lowering the CO_2 concentration in the environment, our approach can also be utilized in tandem removal of other toxic aquatic pollutants such as toxic heavy metal ions, allowing simultaneous adsorption of multiple pollutants toward overall water remediation. This work promises to open up new avenues toward designing functional materials for dissolved CO_2 capture from water and significant advancements toward Sustainable Development Goals.

Methods

Synthesis. All the necessary organic ligands and MOFs were synthesized following the already reported protocols. Detailed discussion about the synthesis of MOFs and organic ligands are included in the Supporting Information file: section 3.

MOF characterization. The crystallinity of MOF structures was confirmed by powder X-ray diffraction using the D8 Advance Diffractometer (Bruker) with the copper $K_{\alpha 1}$ radiation (λ = 1.5406 Å) in the 2θ range of 6−80°, using a 0.05° step size per 1 s at RT. The thermogravimetric properties of MOFs were analysed using a Setsys 1200 apparatus (Setaram) over the temperature range of 30−900°C at a constant rate of 10°C/min under 100 cm^3/min flow of N_2 gas. Scanning electron microscopic images were acquired with a Hitachi S-4800 scanning electron microscope (150 s, 20 mA, 10 kV, zoom at ×10.000) while the samples were subjected to a thin gold coating on the top. Infrared spectra of MOFs were acquired using an FTIR Bruker IFS 66v/S 161 spectrometers in transmission mode in a wavenumber range of 400−4000 cm^{-1}. Low-temperature gas adsorption experiments were executed on a Quantachrome Autosorb-iQ MP gas sorption analyzer 1 atm in a liquid nitrogen (-196 °C) bath. Prior to measurements, powder samples (100−250 mg) were heated at 180 °C for 2 h and outgassed to 10^{-3} Torr.

Carbonic acid species capture from water solutions. As CO_2 molecules dissolve and react in water to form various carbonic acid depending upon the pH of the medium, the Total Carbon (TC), Total Organic Carbon (TOC), and Total Inorganic Carbon (TIC) concentration in the liquid phase was estimated using a TOC-L analyzer (Shimadzu; Japan) via catalytic high-temperature combustion, equipped with an additional nondispersive infrared (NDIR) sensor for specific CO_2 detection. The catalytic oxidation of stock solutions was carried out via combustion at 680°C inside the tubes filled with platinum catalyst. TC and TOC values were measured directly via the TOC-L analyzer with solutions before/after the adsorption of inorganic carbon species to MOFs. All pH measurements were performed with the use of (1) an Aqualytic Portable meter AL10pH (Germany) in Poznan, (2) a pH 1100 L (VWR, the Netherlands) at Utrecht, or (3) a Seven Easy pH meter (Mettler Toledo; Ohio, USA) at Munich, which was calibrated by buffer solution of pH 4.01, pH 7.00 and pH 9.21. Inductively coupled plasma optical emission

spectrometry (ICP-OES; ICPE-9820 with mini-torch; Shimadzu, Japan) was applied for qualitative and quantitative detection of elements (Na, K, Rb, Cs, Mg, Ca, Th, In, S, P, B, Al) in the collected water samples.

Advanced characterization by vibrational spectroscopy. *In situ* Fourier transform-infrared (FTIR) spectroscopy was utilized to monitor the sorption process of CO_2 and carbonate species in both gas and liquid phase with a Perkin Elmer 3 FTIR spectrometer with N_2-cooled MCT detector in attenuated total reflection (ATR) mode. ATR crystals (20 x 10 x 0.5 mm, 45°) cut from double side polished Si wafer and a depth of penetration d_p = 0.52 µm (at 1600 cm^{-1}) and an effective pathlength of $d_{e\parallel}$ =0.64 µm $d_{e\perp}$ =0.32 µm, yielding at total effective pathlength of $(d_{e\parallel}+d_{e\perp})/2$ * N = 9.65 µm with N = 20 were used. The temperature of the aluminum flow cell was controlled using a thermoelectric cooling (TEC) controller (TEC-1091, Meerstetter, Switzerland) and a 20 x 20 mm Peltier element (RS components, the Netherlands). MOF films were obtained by drop casting MOF suspensions (2 mg MOF powder in 100 µL methanol) onto the ATR crystal and subsequent heating to 80°C for 30 min. Carbonate solutions were applied with 1.5 mL min^{-1} flow using a peristaltic pump (Ismatec, Germany) and 1/16" PFA tubing.

References

1. Boyd, P. G. *et al.* Data-driven design of metal-organic frameworks for wet flue gas CO_2 capture, *Nature*, **576**, 253–256, (2019).

2. Ruddiman, W.F. *et al.* The early anthropogenic hypothesis: a review, *Quat. Sci. Rev.*, **240**, 106386, (2020).

3. Rothenberg, G. *et al.* A realistic look at CO_2 emissions, climate change and the role of sustainable chemistry, *Sustain. Chem. Clim. Action*, **2**, 100012, (2023).

4. Zhang, L. *et al.* Nanostructured Materials for Heterogeneous Electrocatalytic CO_2 Reduction and their Related Reaction Mechanisms. *Angew. Chem. Int. Ed.*, **56**, 11326–11353, (2017).

5. Mikkelsen, M. *et al.* The teraton challenge. A review of fixation and transformation of carbon dioxide. *Energy Environ. Sci.*, **3**, 43–81, (2010).

6. Gruber, N. *et al.* The oceanic sink for anthropogenic CO_2 from 1994 to 2007. *Science*, **363**, 1193–1199, (2019).

7. McDonald, T. M. *et al.* Cooperative insertion of CO_2 in diamine-appended metal-organic frameworks. *Nature*, **519**, 303–308, (2015).

8. Bronselaer, B. *et al.* Heat and carbon coupling reveals ocean warming due to circulation changes. *Nature*, **584**, 227–233, (2020).

9. Hurd, C. L. *et al.* Current understanding and challenges for oceans in a higher-CO_2 world. *Nat. Clim. Change*, **8**, 686–694, (2018).

10. Intergovernmental Panel on Climate Change (ipcc). Climate Change 2013: The Physical Science Basis. Contribution of Working Group I to the Fifth Assessment Report of the Intergovernmental Panel on Climate Change, (2013).

11. Doney, S. C. *et al.* Ocean acidification: the other CO_2 problem. *Annu. Rev. Mar. Science*, **1,** 169−192, (2009).

12. Feely, R. A. *et al.* Ocean Acidification: The Other CO_2 Problem. *Limnol. Oceanogr. e-Lect.,* (2011).

13. Orr, J. C. *et al.* Anthropogenic ocean acidification over the twenty-first century and its impact on calcifying organisms. *Nature*, **437,** 681−686, (2005).

14. Pelejero, C. *et al.* Paleo-perspectives on ocean acidification. *Trends in ecology & evolution*, **25,** 332−344, (2010).

15. Boot-Handford, M. E. *et al.* Carbon capture and storage update. *Energy Environ. Sci.*, **7,** 130−189, (2014).

16. Oschatz, M. *et al.* A search for selectivity to enable CO 2 capture with porous adsorbents. *Energy Environ. Sci.*, **11,** 57−70, (2018).

17. Flaig, R. W. *et al.* The Chemistry of CO2 Capture in an Amine-Functionalized Metal-Organic Framework under Dry and Humid Conditions. *J. Am. Chem. Soc.*, **139,** 12125−12128, (2017).

18. Sumida, K. *et al.* Carbon dioxide capture in metal-organic frameworks. *Chem. Rev.*, **112,** 724−781, (2012).

19. Yu, J. *et al.* CO_2 Capture and Separations Using MOFs: Computational and Experimental Studies. *Chem. Rev.*, **117,** 9674−9754, (2017).

20. Banerjee, R. *et al.* High-throughput synthesis of zeolitic imidazolate frameworks and application to CO_2 capture. *Science*, **319,** 939−943, (2008).

21. Chen, K.-J. *et al.* Efficient CO_2 Removal for Ultra-Pure CO Production by Two Hybrid Ultramicroporous Materials. *Angew. Chem. Int. Ed.*, **57,** 3332−3336, (2018).

22. Kim, E. J. *et al.* Cooperative carbon capture and steam regeneration with tetraamine-appended metal-organic frameworks. *Science*, **369,** 392−396, (2020).

23. Lin, L.-C. *et al.* Understanding CO_2 dynamics in metal-organic frameworks with open metal sites. *Angew. Chem. Int. Ed.*, **52,** 4410−4413, (2013).

24. Chae, H. K. *et al.* A route to high surface area, porosity and inclusion of large molecules in crystals. *Nature*, **427,** 523−527, (2004).

25. Furukawa, H. *et al.* Ultrahigh porosity in metal-organic frameworks. *Science*, **329,** 424−428, (2010).

26. Hirai, K. *et al.* Sequential functionalization of porous coordination polymer crystals. *Angew. Chem. Int. Ed.*, **50,** 8057−8061, (2011).

27. Wang, K. *et al.* A series of highly stable mesoporous metalloporphyrin Fe-MOFs. *J. Am. Chem. Soc.*, **136,** 13983−13986, (2014).

28. Mukherjee, S. *et al.* Advances in adsorptive separation of benzene and cyclohexane by metal-organic framework adsorbents. *Coord. Chem. Rev.*, **437,** 213852, (2021).

29. Rieth, A. J. *et al.* Kinetic stability of metal−organic frameworks for corrosive and coordinating gas capture. *Nat. Rev. Mater.*, **4,** 708−725, (2019).

30. Takashima, Y. *et al.* Molecular decoding using luminescence from an entangled porous framework. *Nat. Commun.*, **2,** 168, (2011).

31. Jaramillo, D. E. *et al.* Ambient-Temperature Hydrogen Storage via Vanadium(II)-Dihydrogen Complexation in a Metal-Organic Framework. *J. Am. Chem. Soc.*, **143,** 6248−6256, (2021).

32. Mason, J. A. *et al.* Methane storage in flexible metal-organic frameworks with intrinsic thermal management. *Nature*, **527,** 357−361, (2015).

33. Ding, M. *et al.* Carbon capture and conversion using metal-organic frameworks and MOF-based materials. *Chem. Soc. Rev.*, **48,** 2783−2828, (2019).

34. Rojas, S. *et al.* Metal-Organic Frameworks for the Removal of Emerging Organic Contaminants in Water. *Chem. Rev.*, **120,** 8378−8415, (2020).

35. Zhu, L. *et al.* Identifying the Recognition Site for Selective Trapping of $^{99}TcO_4^-$ in a Hydrolytically Stable and Radiation Resistant Cationic Metal-Organic Framework. *J. Am. Chem. Soc.*, **139,** 14873−14876, (2017).

36. Grape, E. S. *et al.* Removal of pharmaceutical pollutants from effluent by a plant-based metal−organic framework. *Nat Water*, **1**, 433−442, (2023).

37. Wongsakulphasatch, S. *et al.* Effect of Fe open metal site in metal-organic frameworks on post-combustion CO_2 capture performance. *Greenhouse Gas Sci. Technol.*, **7,** 383−394, (2017).

38. Li, B. *et al.* Enhanced Binding Affinity, Remarkable Selectivity, and High Capacity of CO_2 by Dual Functionalization of a rht-Type Metal-Organic Framework. *Angew. Chem. Int. Ed.*, **124,** 1441−1444, (2012).

39. Caskey, S. R. *et al.* Dramatic tuning of carbon dioxide uptake via metal substitution in a coordination polymer with cylindrical pores. *J. Am. Chem. Soc.*, **130,** 10870−10871, (2008).

40. Koutsianos, A. *et al.* A new approach to enhancing the CO_2 capture performance of defective UiO-66 via post-synthetic defect exchange. *Dalton Trans.*, **48,** 3349−3359, (2019).

41. Huang, A. *et al.* Microwave-assisted synthesis of well-shaped UiO-66-NH2 with high CO_2 adsorption capacity. *Mater. Res. Bull.*, **98,** 308−313, (2018).

42. Roztocki, K. *et al.* Combining In Situ Techniques (XRD, IR, and ^{13}C NMR) and Gas Adsorption Measurements Reveals CO_2-Induced Structural Transitions and High CO_2/CH_4 Selectivity for a Flexible Metal-Organic Framework JUK-8. *ACS Appl. Mater. Interfaces*, **13,** 28503−28513, (2021).

43. Yu, C. *et al.* Selective capture of carbon dioxide from humid gases over a wide temperature range using a robust metal−organic framework. *Chem. Eng. J.*, **405,** 126937, (2021).

44. Pedersen, O. *et al.* Underwater photosynthesis of submerged plants - recent advances and methods. *Front. Plant Sci.*, **4,** 140, (2013).

45. Jia, M. *et al.* Vapor-assisted self-conversion of basic carbonates in metal-organic frameworks. *Nanoscale*, **13,** 5069−5076, (2021).

46. Kandiah, M. *et al.* Synthesis and Stability of Tagged UiO-66 Zr-MOFs. *Chem. Mater.*, **22,** 6632−6640, (2010).

47. Pokrovski, K. *et al.* Investigation of CO and CO_2 Adsorption on Tetragonal and Monoclinic Zirconia. *Langmuir*, **17,** 4297–4303, (2001).

48. Buchholz, M. *et al.* Carbon dioxide adsorption on a ZnO(101combining macron0) substrate studied by infrared reflection absorption spectroscopy. *Physical chemistry chemical physics : PCCP*, **16,** 1672–1678, (2014).

49. Saussey, J. *et al.* Infrared study of CO_2 adsorption on ZnO. Adsorption sites. *J. Chem. Soc., Faraday Trans. 1*, **78,** 1457, (1982).

50. Choe, J. H. *et al.* MOF-74 type variants for CO_2 capture. *Mater. Chem. Front.*, **5,** 5172-5185 (2021).

51. Chevreau, H. *et al.* Synthesis of the biocompatible and highly stable MIL-127(Fe): from large scale synthesis to particle size control. *CrystEngComm*, **18**, 4094-4101 (2016).

52. Wu, H *et al.* Cu-TDPAT, an rht-Type Dual-Functional Metal−Organic Framework Offering Significant Potential for Use in H_2 and Natural Gas Purification Processes Operating at High Pressures. *J. Phys. Chem. C,* **116, 31**, 16609−16618 (2012).

53. Socrates, G. *Infrared and Raman Characteristic Group Frequencies: Tables and Charts, 3rd Edition | Wiley*. (Wiley, 2004).

54. Socrates, G. *et al.* (2004). *Infrared and Raman Characteristic Group Frequencies: Tables and Charts, 3rd Edition | Wiley(3rd edition). Wiley.*

55. Yu, J. *et al.* CO_2 Capture and Separations Using MOFs: Computational and Experimental Studies, *Chem. Rev.*, **117**, **14**, 9674−9754 (2017).

56. Trickett, C *et al.* The chemistry of metal−organic frameworks for CO_2 capture, regeneration and conversion. *Nat. Rev. Mater.*, **2**, 17045 (2017).

57. Lyu, H *et al.* Carbon Dioxide Capture Chemistry of Amino Acid Functionalized Metal−Organic Frameworks in Humid Flue Gas, *J. Am. Chem. Soc.*, **144**, **5**, 2387−2396 (2022).
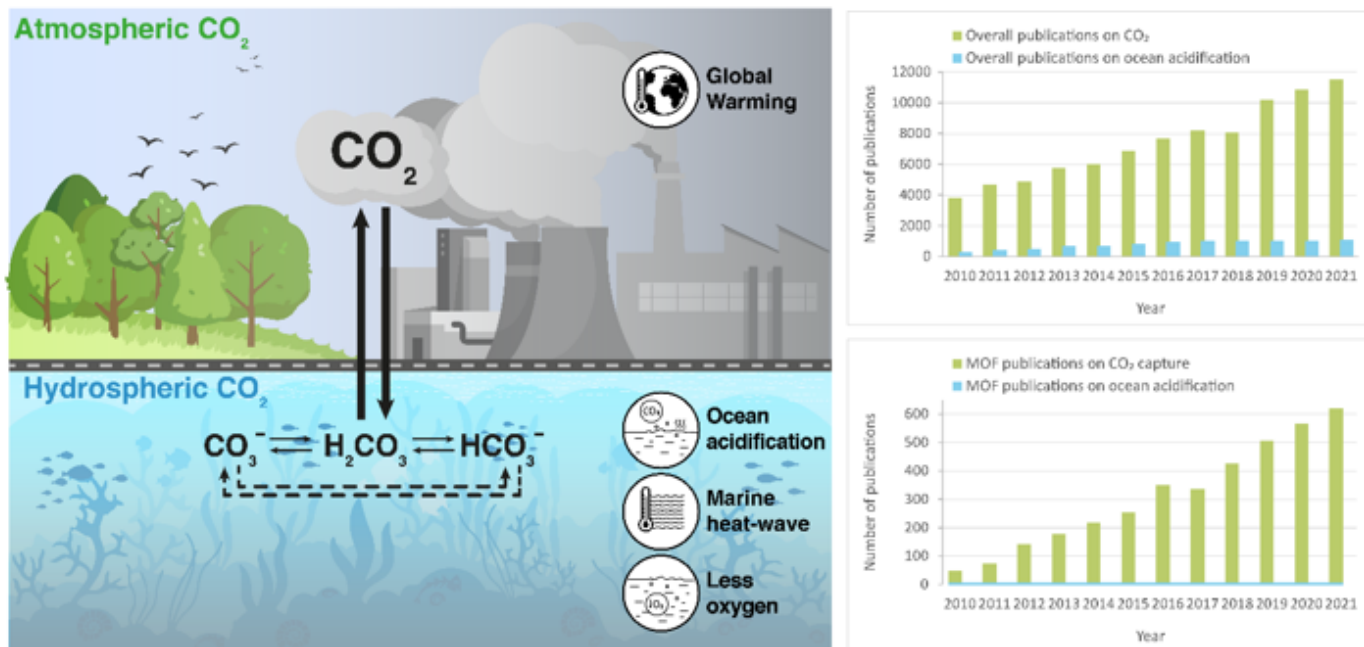
Figures

Figure 1

Overview of the impact of CO_2 on the atmosphere and hydrosphere. (a) Schematic representation of synergic CO_2 cycling between air and sea and its impact on both systems. (b-c) Statistical data between 2005 and today summarizing the scientific contribution toward addressing CO_2 removal issues from the atmosphere and hydrosphere (Source: Web of Science). (b) Statistics on the number of publications on atmospheric CO_2 capture (green) and ocean acidification (blue). (c) Statistics on the number of publications on MOF used for atmospheric CO_2 capture (green) and for ocean acidification (blue).
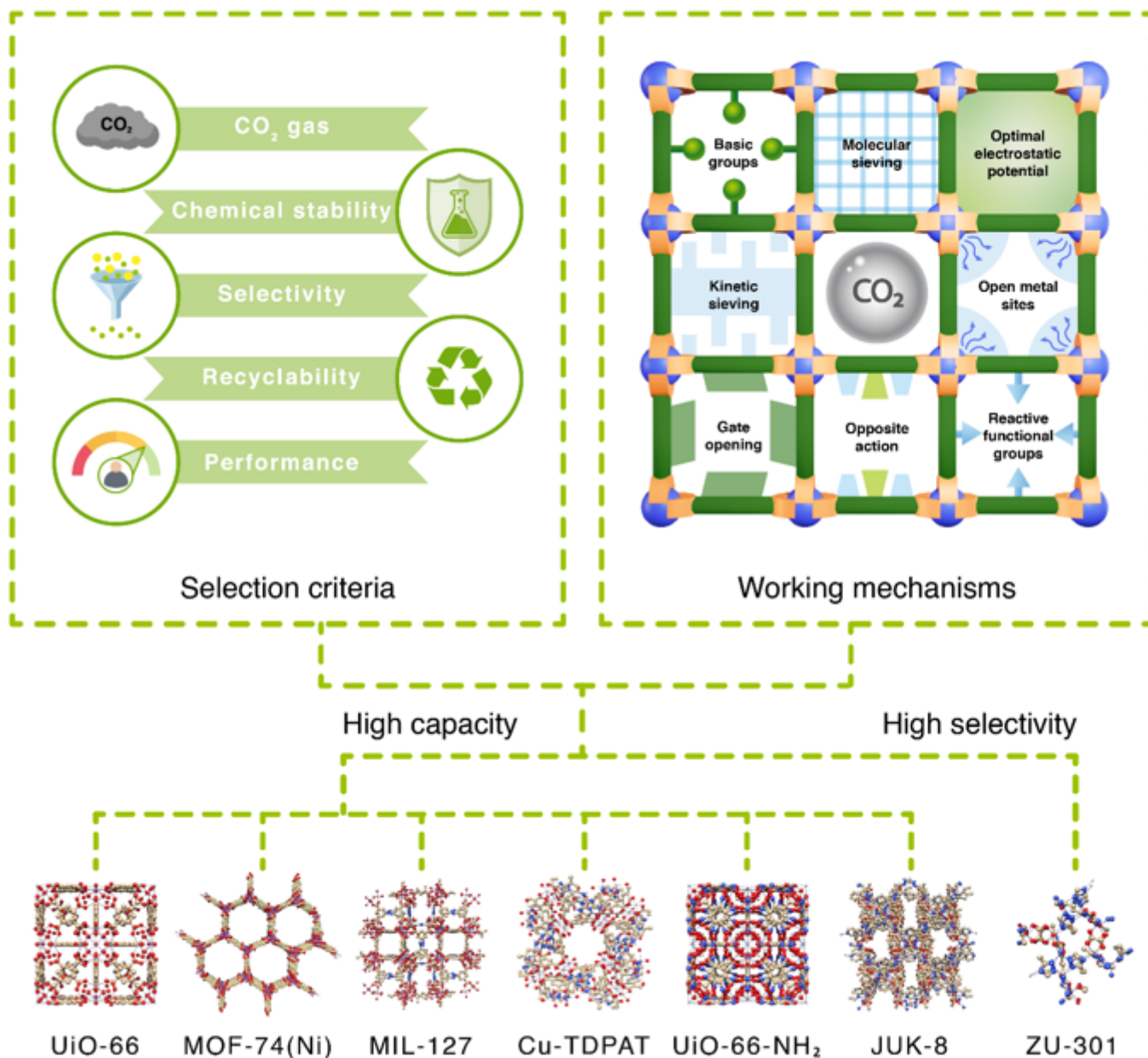
Figure 2

Selection criteria of MOFs offering various CO_2 interaction mechanisms and the seven selected MOFs showing either high atmospheric CO_2 capacity or selectivity.
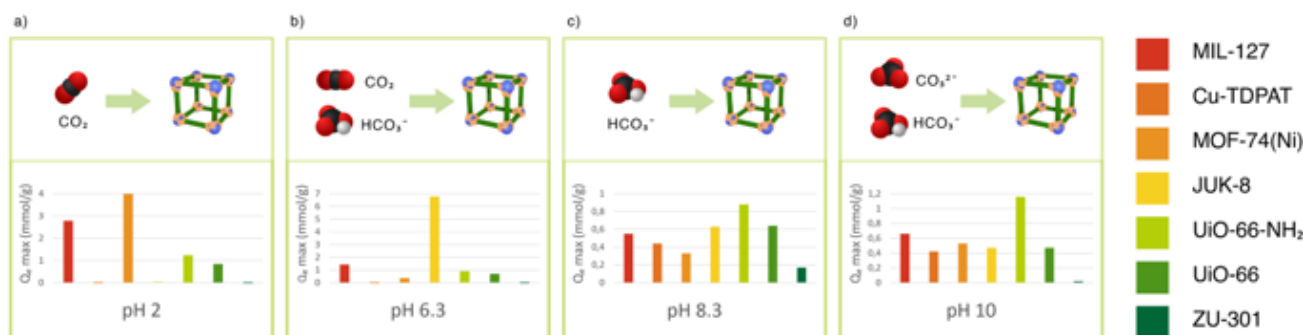
Figure 3

Saturation uptake capacities of the MOFs toward CO_2 and carbonate species at different pHs.
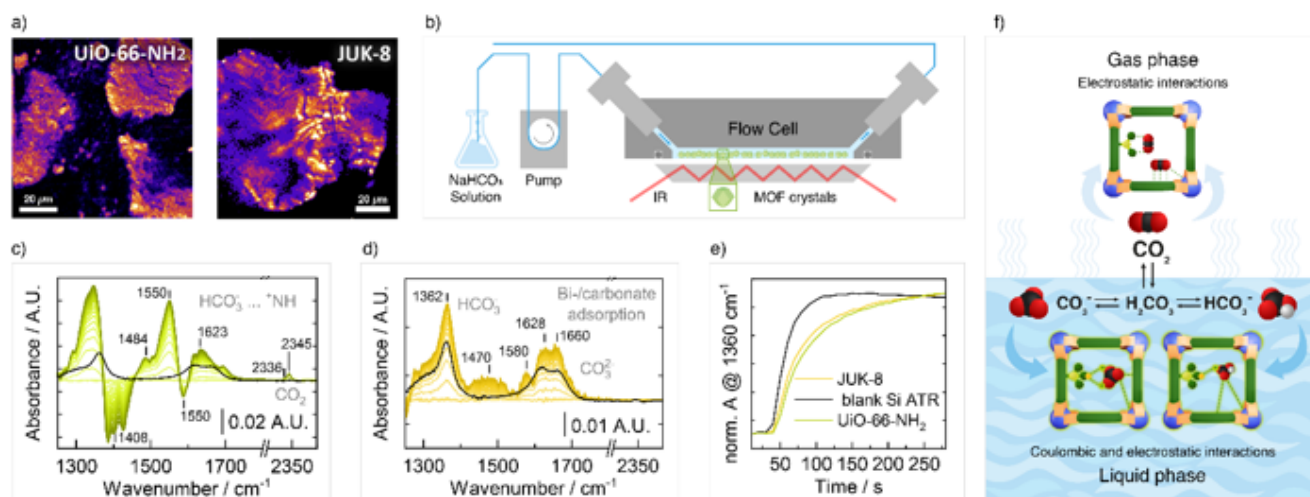**(a)** pH = 2. **(b)** pH = 6.3. **(c)** pH = 8.3. **(d)** pH = 10.

Figure 4

Spectroscopic evaluation of CO_2 adsorption by UiO-66-NH$_2$ and JUK-8 in an aqueous environment. (a) Two-photon excitation-induced fluorescence microscopy reveals that UiO-66-NH$_2$ particles are formed by aggregated nanoparticles while JUK-8 was synthesized as large-sized crystals. (b) Schematic ATR-FTIR experiment to follow CO_2 adsorption to MOFs in solution by transient spectroscopy. (c-d) Difference ATR-FTIR spectra after the addition of 150 mM $NaHCO_3$ (pH 8.3) to the flow cell show an increased adsorption of carbonate species to the Si ATR crystal coated with (c) UiO-66-NH$_2$ or (d) JUK-8. The reference/background spectrum was recorded in the presence of water in the flow cell. (e) ATR-FTIR spectra were obtained after flushing the flow chamber for 250 sec with 150 mM $NaHCO_3$ solution in the absence and presence of UiO-66-NH$_2$ and JUK-8. A comparable uptake is achieved already after 4 min. (f)

Schematic illustration of the interactions of the MOF scaffold with CO_2 in the gas phase and carbonate species in the liquid phase.
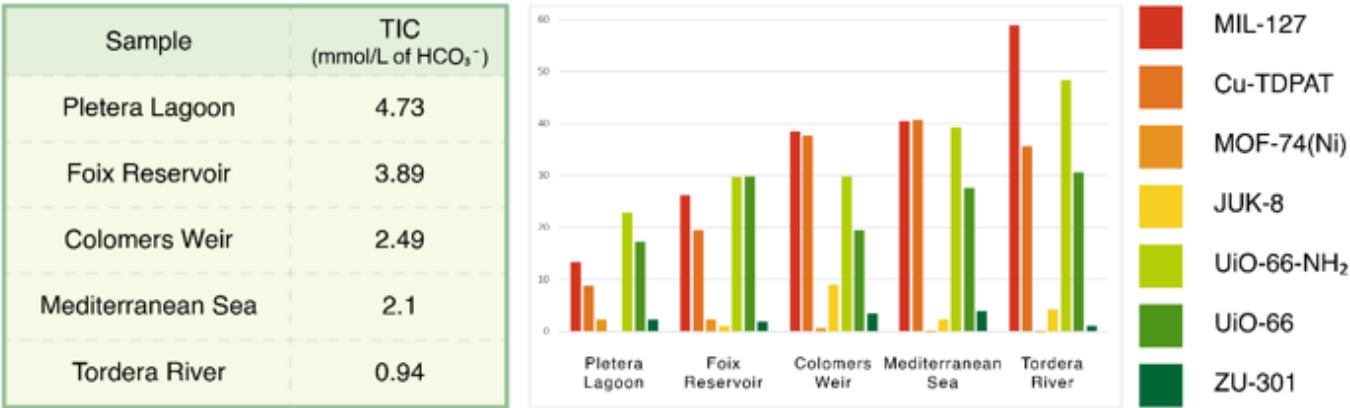

Figure 5

Carbonic acid uptake behavior by MOFs from natural water systems. (left) Amount of total inorganic carbon (TIC) present in the natural water systems. **(right)** Comparison between different MOFs for their total TIC removal performance from different real water samples.

Supplementary Files

This is a list of supplementary files associated with this preprint. Click to download.

- CO2SI.docx.pdf